Alternative splicing of the bicistronic gene molybdenum cofactor synthesis 1 (*MOCS1*) uncovers a novel mitochondrial protein maturation mechanism

Received for publication, August 28, 2019, and in revised form, January 22, 2020 Published, Papers in Press, January 29, 2020, DOI 10.1074/jbc.RA119.010720

Simon J. Mayr[‡], **Juliane Röper**[‡], **and Guenter Schwarz**[‡§1]

From the [‡]*Institute of Biochemistry, Department of Chemistry, University of Cologne, 50674 Cologne, Germany and* [§]*Center for Molecular Medicine, University of Cologne, 5931 Cologne, Germany*

Edited by Ursula Jakob

Molybdenum cofactor (Moco) biosynthesis is a highly conserved multistep pathway. The first step, the conversion of GTP to cyclic pyranopterin monophosphate (cPMP), requires the bicistronic gene molybdenum cofactor synthesis 1 (*MOCS1*). Alternative splicing of *MOCS1* within exons 1 and 9 produces four different N-terminal and three different C-terminal products (type I–III). Type I splicing results in bicistronic transcripts with two open reading frames, of which only the first, *MOCS1A*, is translated, whereas type II/III splicing produces MOCS1AB proteins. Here, we first report the cellular localization of alternatively spliced human MOCS1 proteins. Using fluorescence microscopy, fluorescence spectroscopy, and cell fractionation experiments, we found that depending on the alternative splicing of exon 1, type I splice variants (MOCS1A) either localize to the mitochondrial matrix (exon 1a) or remain cytosolic (exon 1b). MOCS1A proteins required exon 1a for mitochondrial translocation, but fluorescence microscopy of MOCS1AB variants (types II and III) revealed that they were targeted to mitochondria independently of exon 1 splicing. In the latter case, cell fractionation experiments displayed that mitochondrial matrix import was facilitated via an internal motif overriding the N-terminal targeting signal. Within mitochondria, MOCS1AB underwent proteolytic cleavage resulting in mitochondrial matrix localization of the MOCS1B domain. In conclusion, *MOCS1* produces two functional proteins, MOCS1A and MOCS1B, which follow different translocation routes before mitochondrial matrix import for cPMP biosynthesis involving both proteins. MOCS1 protein maturation provides a novel alternative splicing mechanism that ensures the coordinated mitochondrial targeting of two functionally related proteins encoded by a single gene.

The molybdenum cofactor is found in all kingdoms of life forming the active center of molybdenum-containing enzymes, except nitrogenase. In mammals, there are four enzymes that depend on Moco[2]: sulfite oxidase, xanthine oxidase, aldehyde oxidase, and the mitochondrial amidoxime–reducing component (1). Moco is composed of an organic pterin moiety that binds molybdenum via a dithiolene group attached to a pyran ring, which is synthesized by a complex biosynthetic pathway. A mutational block in any step of Moco biosynthesis results in Moco deficiency, a severe inborn error of metabolism characterized by rapidly progressing encephalopathy and early childhood death (2). In recent years, efficient treatment for Moco-deficient patients with a defect in the first step of Moco biosynthesis has been established (3, 4).

Moco biosynthesis is divided into three major steps, starting with GTP followed by the synthesis of three intermediates: cPMP (5), molybdopterin or metal-binding pterin (MPT) (2), and adenylated MPT (6). Because of the strict evolutionary conservation of the pathway, intermediates are identical in all kingdoms of life. The first and most complex reaction sequence is catalyzed by two proteins in bacteria (MoaA and MoaC) whereas in humans different translation products originating from different open reading frames (ORFs) of the *MOCS1* gene (encoding MOCS1A and MOCS1AB proteins) are required for cPMP synthesis (7–9).

Escherichia coli MoaA and mammalian MOCS1A belong to the superfamily of radical S-adenosylmethionine (SAM) proteins with two highly oxygen-sensitive [4Fe-4S] clusters (Fig. 1*A*). The respective reaction mechanism has been studied for MoaA and involves reductive cleavage of SAM by the N-terminal [4Fe-4S] cluster (10). The resulting 5′-deoxyadenosyl radical initiates the transformation of 5′-GTP, which is bound to a C-terminal [4Fe-4S] cluster by abstracting the 3′ proton from the ribose. Following a multistep rearrangement reaction, 3,8′cH$_2$-GTP is released (Fig. 1*B*) (11) and further processed by the second protein (*E. coli* MoaC, respectively human MOCS1AB) (7), resulting in pyrophosphate release and cyclic phosphate formation (Fig. 1*C*) (9, 12).

Interestingly, in the first two steps of Moco biosynthesis (cPMP and MPT synthesis) bicistronic transcripts (*MOCS1* and *MOCS2*) have been reported (8, 13), which is highly unusual in human gene expression (14). Proteins involved in cPMP synthesis are encoded by the *MOCS1* gene harboring 10

This work was supported by Deutsche Forschungsgemeinschaft (DFG) Grant SCHW 759/10-1/2 (to G. S. and S. J. M.) and SFB1218, B08 (to G. S.). The authors declare that they have no conflicts of interest with the contents of this article.

This article contains Figs. S1–S6.

[1] To whom correspondence should be addressed: Zülpicher Str. 47, 50674 Cologne, Germany. Tel.: 49-221-470-6441; Fax: 49-221-470-5092; E-mail: gschwarz@uni-koeln.de.

[2] The abbreviations used are: Moco, molybdenum cofactor; cPMP, cyclic pyranopterin monophosphate; MPT, metal-binding pterin; MPP, mitochondrial processing peptidase; MOCS, molybdenum cofactor synthesis.

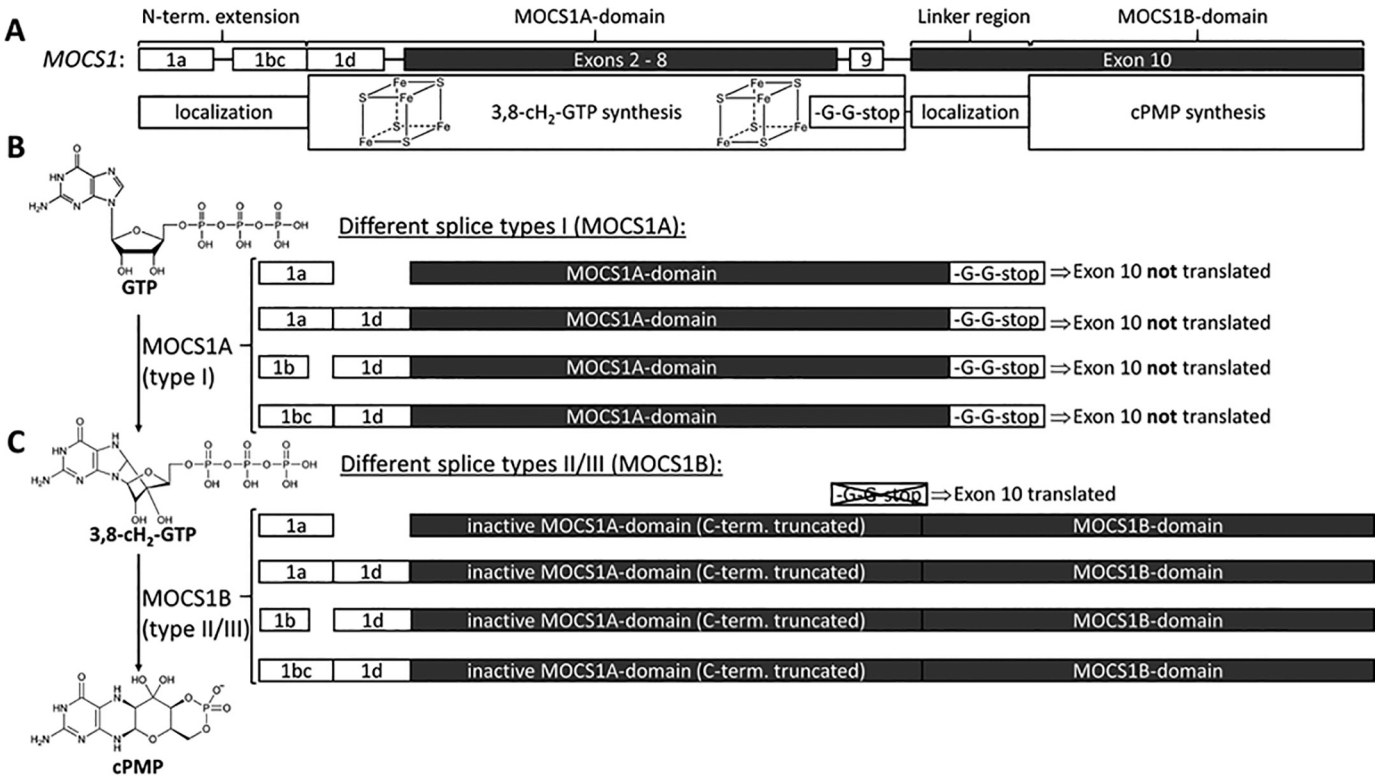

Figure 1. Alternative splicing of the *MOCS1* gene and gene products involved in cPMP synthesis. *A*, exon structure of the *MOCS1* gene highlighting the alternatively spliced exon 1 cassettes (*white boxes*), the shared exons 2–8 (*gray boxes*), the alternatively spliced exon 9 (*white box*), as well as the MOCS1B encoding exon 10 (*white box*). Introns are indicated by a *black line* but are not reflecting actual intron size. Above the gene structure the encoded domains are indicated, whereas below the gene structure encoded features are shown, including the hypothesized localization signals, iron-sulfur cluster–binding sites, the functional biosynthetic domains and the exon 9 encoded double glycin motif followed by the stop codon (-G-G-stop). *B*, different splice type I MOCS1 variants involved in the conversion of GTP to 3,8-cH$_2$-GTP. The splicing of exon 1 creates four alternative N-terminal combinations (*white boxes*), whereas exon 9 is not spliced out leaving the double glycine motif and the stop codon in place. As a consequence active MOCS1A (exons 1–9), but not MOCS1B (exon 10) is translated. *C*, different splice type II/III MOCS1 variants involved in the conversion of 3,8-cH$_2$-GTP to cPMP. The monocistronic type II and III variants on do not contain the double glycine motif and the stop codon by having exon 9 removed either partially (type II) or entirely (type III), resulting in a MOCS1AB fusion protein representing active MOCS1B. Alternative splicing of exon 1 creates the same four different splice combinations as found in splice type I for both splice type II and III.

exons (Fig. 1*A*) leading to different alternatively spliced *MOCS1* transcripts (15). The transcripts are classified into three forms: Type I transcripts are bicistronic mRNAs with two nonoverlapping ORFs, MOCS1A and MOCS1B (16), of which only the first ORF is translated, yielding active MOCS1A (Fig. 1*B*). Type II and III transcripts are derived from two alternative splice sites within exon 9, both resulting in the lack of the MOCS1A stop codon and an in-frame-fusion with the second ORF (MOCS1B), thus producing a monocistronic transcript. Consequently, MOCS1B is not expressed independently yet as a MOCS1AB fusion protein. Splice type II only lacks 15 nucleotides of exon 9, whereas in the type III variant the entire exon 9 is absent. The resulting MOCS1AB fusion proteins harbor an active MOCS1B domain and a catalytically inactive MOCS1A domain because of deletion of the last two residues harboring a conserved and catalytically essential C-terminal double-glycine motif (7) (Fig. 1*C*). Therefore alternative splicing of exon 9 determines whether translation products function as MOCS1A or MOCS1B proteins. Type I and type III variants present 41 and 55% of all MOCS1 transcripts, respectively, the remainder being type II transcripts (17).

In addition to exon 9 alternative splicing, cDNA sequences with four different 5′-regions have been reported and were named after the authors first describing the respective variants. Two alternative ATG start codons are encoded either by exon 1a (present in LARIN and ARENAS variants) or exon 1b (present in REISS and GROSS variants). Because of the lack of an intronic 3′ splice site in LARIN, exon 1a is spliced to exon 1d, although in ARENAS it is directly joined to exon 2 (subsequently referred to as MOCS1-ad and MOCS1-a). In a third REISS variant, exon 1b is joined with exons 1c and 1d, although in GROSS, it is spliced together with exon 1d (MOCS1-bcd and MOCS1-bd) (Fig. 1, *B* and *C*). MOCS1-ad and MOCS1-bcd transcripts were found in different tissues, and expression levels of MOCS1-bd were found to be very low (18).

Compared with their bacterial orthologues, human MOCS1 proteins exhibit exon 1 encoded N-terminal extensions of up to 56 residues depending on the length of the N-terminal splicing product of *MOCS1*. In contrast, in plants two genes (*Cnx2* and *Cnx3*) encode for proteins required for cPMP synthesis, both of which are characterized by extension of up to 112 residues encoding for classical N-terminal mitochondrial targeting signals (19). Therefore, we proposed that MOCS1 proteins also localize to mitochondria and asked the question how alternative splicing of *MOCS1* transcripts controls the function and localization of MOCS1 proteins (Fig. 1*A*).

We found that in the bicistronic *MOCS1* transcripts (MOCS1A) exon 1 splicing results in translocation to the mito-

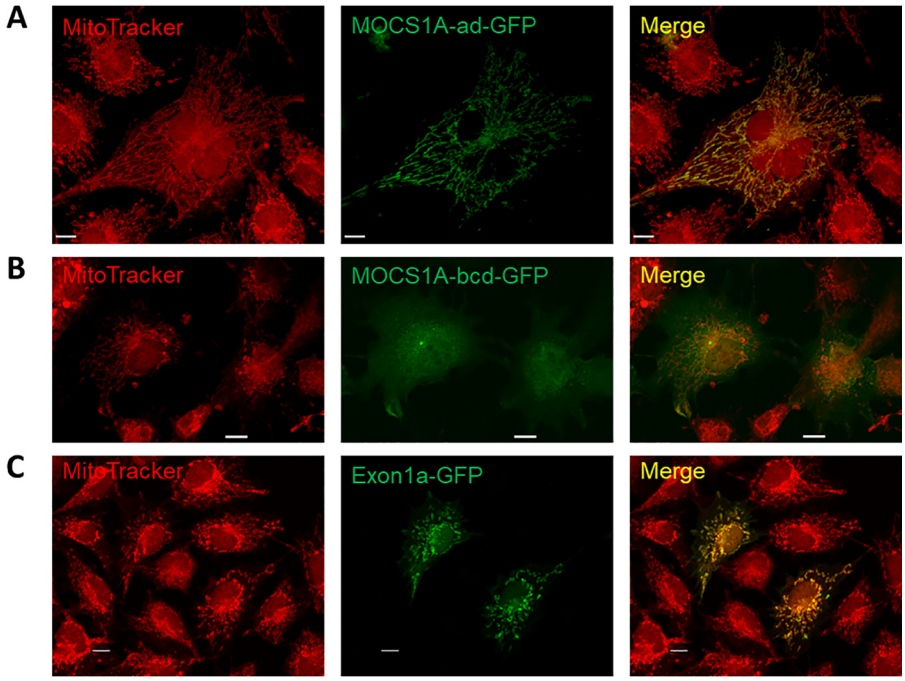

Figure 2. Transient expression of MOCS1A splice variants and MOCS1-derived constructs as GFP fusions in COS7 cells. *A–C*, COS7 cells were transfected with (*A*) MOCS1A-ad, (*B*) MOCS1A-bcd, and (*C*) exon 1a. Following 48 h of transient expression, mitochondria were stained with MitoTracker® Red CMXRos and analyzed by confocal laser scanning microscopy (three independent experiments). Overlay between the *red* and *green* (GFP) channel is shown in the *yellow* merge panel. *Scale bars*: 10 μm.

chondrial matrix when exon 1a is translated, whereas exon 1b variants remain cytosolic. In contrast, all monocistronic transcripts (MOCS1AB) produced proteins that were imported into mitochondria, regardless of their exon 1 composition. Additional sub-mitochondrial localization studies of the MOCS1AB proteins revealed that only the proteolytic MOCS1B cleavage product was imported into the mitochondrial matrix, and full-length MOCS1AB could only be witnessed on the outer mitochondrial membrane.

Results

Localization of MOCS1A proteins

Given the N-terminal extension of the MOCS1 proteins compared with the homologous bacterial MoaA protein, first the different N-terminal splice variants were investigated concerning their cellular localization, knowing that N-terminal extensions may be involved in cellular translocation processes. Based on the published sequences for MOCS1-a (17), MOCS1-ad (AF034374) (20), MOCS1-bd (18), and MOCS1-bcd (13) variants, the four exon 1 type I splice variants were created by fusion PCR and inserted into pEGFP-N1. Subsequently constructs were expressed in COS7 cells as EGFP fusion proteins. Although the MOCS1A-ad–EGFP protein colocalized with the mitochondrial marker (MitoTracker®) (Fig. 2*A*), a diffuse cytosolic distribution was observed for MOCS1A-bcd–EGFP (Fig. 2*B*), suggesting that exon 1a facilitates mitochondrial import, given that exon 1d and exons 2–9 are shared between MOCS1A-ad and MOCS1A-bcd. In accordance, no difference in cellular localization between MOCS1A-a and MOCS1A-ad could be observed, whereas MOCS1A-bd in contrast to MOCS1A-bcd formed aggregates not colocalized with mitochondria in the cells (Fig. S1).

To probe the role of exon 1a in the mitochondrial targeting of MOCS1A, exon 1a was expressed as an EGFP fusion protein in COS7 cells also resulting in colocalization with the mitochondrial marker (Fig. 2*C*). Following *in silico* analysis of the MOCS1A-ad sequence for mitochondrial translocation signals (MitoProtII) (21) revealed a high mitochondrial import probability (99.94%) and a cleavage site after 22 residues (Fig. 3*A*). Subsequent expression of a fusion protein consisting of the N-terminal 22 residues and EGFP indeed resulted in colocalization of EGFP and the mitochondrial marker (Fig. 3*B*), confirming the presence of a classical N-terminal import signal in exon 1a. *In silico* analysis of the MOCS1A-ad sequence using HeliQuest (22) revealed the formation of an amphipathic helix within the N-terminal 22 residues between Arg-4 and Cys-21 (Fig. 3*A*).

MOCS1A proteins harbor two [4Fe-4S], of which the N-terminal cluster is coordinated by two cysteines encoded by exon 1d. Expression of all four MOCS1A isoforms yielded in comparable activities of all splice variants except MOCS1A-a, which showed strongly reduced activity as expected because of the absence of exon 1d (Fig. S2). This finding underlines the importance of fully coordinated [4Fe-4S] clusters limiting the localization of MOCS1A to certain cellular compartments, such as the mitochondrial matrix (23). To probe for matrix import of MOCS1A-ad, we expressed MOCS1A-ad in HEK293 cells and enriched mitochondria after 2 days of culture. Enriched mitochondria were resuspended in two different buffers, one either keeping the mitochondria stable or inducing hypotonic swelling causing disruption of the outer mitochondrial membrane. Addition of proteinase K to mitochondria of each condition revealed that proteinase K was not able to digest MOCS1A-ad in both intact and swollen mitochondria (Fig. 3*C*), indicating

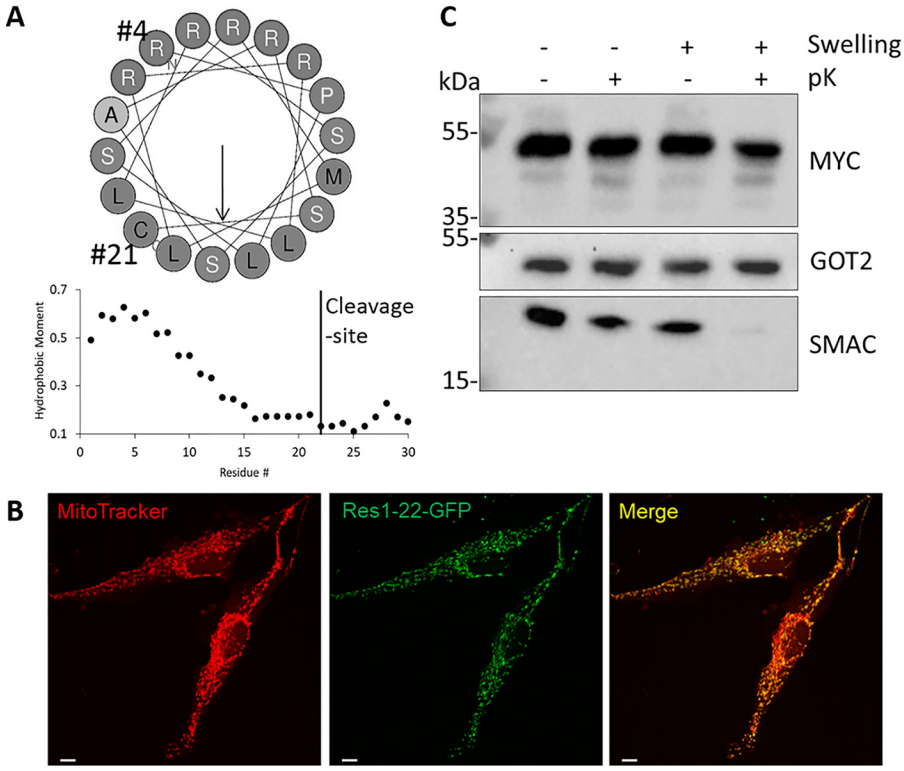

Figure 3. Mitochondrial import of MOCS1A. *A*, prediction of N-terminal amphipathic helix consisting of the residues 4 to 21 encoded by exon 1a (HeliQuest). *B*, transient expression of residues 1–22 encoded by exon 1a as GFP fusions in COS7 cells. Following 48 h of transient expression, mitochondria were stained with MitoTracker® Red CMXRos and analyzed by confocal laser scanning microscopy (three independent experiments). Overlay between the *red* and *green* (GFP) channel is shown in the *yellow* merge panel. *Scale bars*: 10 μm. *C*, partial proteolysis experiment of mitochondria enriched from HEK293 cells overexpressing MYC-tagged MOCS1A-ad (46.2 kDa). One of each fraction of intact and swollen mitochondria were treated with proteinase K. Subsequent 10% SDS-PAGE followed by Western blot analysis was performed using anti-MYC, anti-SMAC, and anti-GOT2 antibodies.

mitochondrial matrix localization. This was confirmed by the efficient digestion of SMAC protein (IMS loading control) in the proteinase K–treated swollen mitochondria sample, but not of GOT2 protein (matrix loading control). As a result, MOCS1A was found to be translocated to the mitochondrial matrix via a classical mitochondrial targeting signal located in exon 1a.

Localization of MOCS1AB proteins

Based on the results obtained for MOCS1A proteins, we subsequently investigated the cellular localization of MOCS1AB proteins (splice type III, encoded by exons 1–8 and exon 10). Similar to the experimental design for MOCS1A proteins, we expressed MOCS1AB-ad–EGFP and MOCS1AB-bcd–EGFP in COS7 cells. As expected, MOCS1AB-ad–EGFP colocalized with the mitochondrial marker (Fig. 4*A*); however, when we expressed the MOCS1AB-bcd–EGFP fusion protein we also observed mitochondrial localization (Fig. 4*B*), even though exon 1a–encoded residues were not present. Testing splice type II variants resulted in mitochondrial localization independent of exon 1 composition as well (Fig. S3). Because the exons 1–8 are shared between the type I (MOCS1A) and type III (MOCS1AB) splice variants, our finding suggested the presence of an additional translocation signal encoded by exon 10.

Alignment of MOCS1AB with the homologous bacterial proteins MoaA and MoaC revealed a polypeptide sequence of 95 nonconserved residues located between the MOCS1A and MOCS1B domain, encoded by the 5′ sequence of exon 10 (Fig. 4*C*). Such a sequence outside the functional domain might indicate an internal translocation signal, which was indeed confirmed by stepwise TargetP *in silico* sequence analysis (24, 25). Furthermore, subsequent HeliQuest sequence analysis showed the presence of an amphipathic helix resulting in a hydrophobic moment at position 395 (22) (Fig. 5*A*). To probe this bioinformatic approach, full-length exon 10 (representing MOCS1B) and a deletion of the 5′ 285 bases of exon 10 (representing MOCS1BΔ1–95 residues) were expressed in HEK293 cells using a pCDNA3.1 vector. To ensure that neither an N-terminal nor a C-terminal translocation signal would be disturbed, no tags were fused to the construct, but an antibody was raised against recombinant MOCS1BΔ1–95. HEK293 cells were harvested after 2 days of protein expression and fractionated into cytosolic (mitochondria free) and noncytosolic fraction (containing mitochondria). Comparative Western blot analysis of the obtained fractions revealed a strong enrichment of MOCS1B to the noncytosolic fraction whereas the majority of MOCS1BΔ1–95 was retained in the cytosolic fraction, confirming the presence of an internal translocation signal at the N-terminus of MOCS1B (Fig. 5*B*), which was in accordance with the loading controls VDAC (mitochondria) and gephyrin (cytosol). The cellular distribution of both MOCS1B variants was subsequently confirmed by transfecting COS7 cells with plasmids expressing both exon 10 and exon 10Δ1–285 as EGFP fusion proteins. Although the MOCS1B(exon 10)–EGFP fusion protein again localized to mitochondria (Fig. 5*C*), we found that

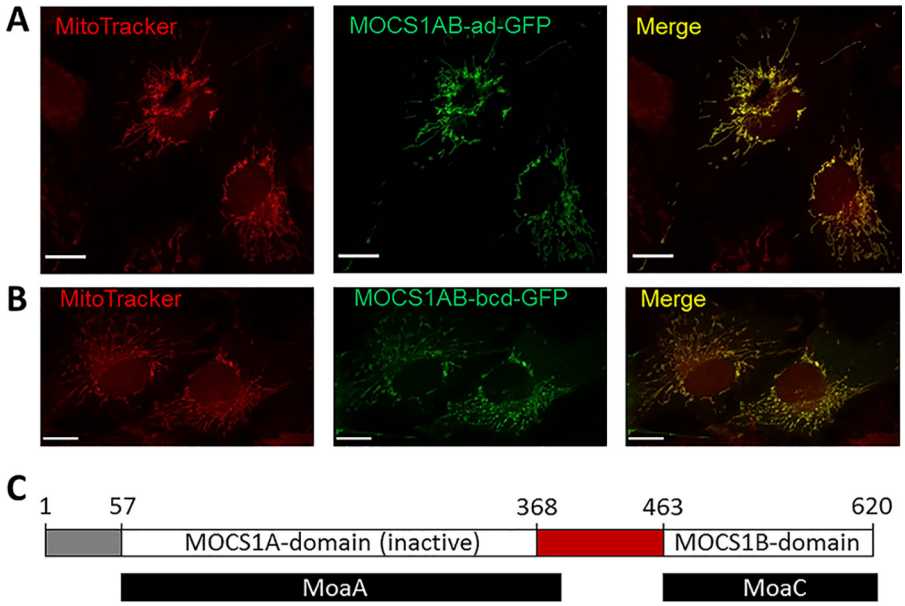

Figure 4. Identification of internal translocation signal of MOCS1AB proteins. *A* and *B*, transient expression of MOCS1AB splice variants (type III) as GFP fusions in COS7 cells. COS7 cells were transfected with (*A*) MOCS1AB-ad and (*B*) MOCS1A-bcd. Following 48 h of transient expression, mitochondria were stained with MitoTracker® Red CMXRos and analyzed by confocal laser scanning microscopy (three independent experiments). Overlay between the *red* and *green* (GFP) channel is shown in the *yellow* merge panel. *Scale bars*: 10 μm. *C*, alignment of MOCS1AB (*white box*) with *E. coli* MoaA and MoaC (*black boxes*). Numbers indicate the positions of residues defining the N-terminal extension (*gray box*) and the internal extension (*red box*).

the MOCS1BΔ1–95(exon 10Δ1–285)–EGFP fusion showed a cytosolic distribution of the protein (Fig. 5*D*), demonstrating indeed the presence of an additional translocation signal in the exon 10 encoded linker region connecting the MOCS1A and MOCS1B domains.

Sub-mitochondrial localization of MOCS1AB

Considering that MOCS1A proteins are either cytosolic or mitochondrial matrix proteins, we next investigated the sub-mitochondrial localization of MOCS1AB proteins and whether this is influenced by their exon 1 composition. Therefore we first compared the mitochondrial distribution of MOCS1A-ad and MOCS1AB-bcd by expressing both proteins as N-terminal fusions to ratiometric pHluorin (26) in HEK293 cells. First we calibrated the ratiometric pHluorin protein to different pH values. Cells were harvested and fractionated and finally the non-cytosolic fractions were resuspended in buffers of different known pH values and disrupted, resulting in excitation spectra differing in their excitation maxima at 388 nm and 456 nm in a ratiometric manner (Fig. 6*A*). As a result, the excitation peak at 388 nm was rising with increasing pH, whereas the signal at 456 nm was decreasing accordingly. The ratio of the excitation bands (388 nm/456 nm) was then related to the respective pH values and a sigmoidal fit curve was applied (Fig. 6*B*), allowing the calculation of an unknown pH value from determined excitation ratios.

Subsequently, both MOCS1A-ad–pHluorin and MOCS1AB-bcd–pHluorin were expressed in HEK293 cells, harvested, and fractionated. The noncytosolic fraction was again resuspended in a buffer of known pH (7.4), but was left intact. Measurement of the intact mitochondria yielded pH values of 7.78 ± 0.02 for MOCS1A-ad and 7.90 ± 0.03 for MOCS1AB-bcd indicating matrix localization for both proteins when compared with the mitochondrial matrix protein GOT2 (7.86 ± 0.05). Following the measurement of the intact mitochondria, samples were disrupted and remeasured, resulting in the expected pH values of 7.41 ± 0.05 and 7.28 ± 0.02 for MOCS1A-ad and MOCS1AB-bcd resembling the pH of the used buffer and differing from the pH of the intact mitochondria significantly (Fig. 6*C*). The pHluorin determined pH values furthermore exclude translocation of MOCS1 proteins to other cell organelles such as endoplasmic reticulum, Golgi apparatus, or lysosomes, given that they all display pH values below 7.4 (27).

In addition to the ratiometric pHluorin studies, localization of MOCS1A-ad and MOCS1AB-bcd protein to the mitochondrial matrix strongly suggested matrix localization of MOCS1AB-ad as well. To confirm this proposal, MOCS1AB-ad was expressed in HEK293 cells without any tag using the pCDNA3.1 vector. Following enrichment of mitochondria the aforementioned proteinase K treatment was performed. Surprisingly MOCS1AB could not be detected by the MOCS1B antibody in either sample that was exposed to proteinase K, but it was present in both control samples (Fig. 6*D*), suggesting that MOCS1AB is localized to the outer side of the outer mitochondrial membrane. The experiment was also repeated using EGFP-fused MOCS1AB-bcd (Fig. S4), with a similar result indicating that neither the EGFP nor the pHluorin tag, nor the exon 1 composition alters the translocation of MOCS1AB proteins. This finding was in contrast to the obtained results of the pHluorin measurements.

However, in addition to the bands observed for the full-length MOCS1AB proteins, the MOCS1B antibody also detected a band at ~20 kDa in both proteinase K–treated samples as well as untreated samples, but not in a control sample of disrupted mitochondria treated with proteinase K (Fig. 6*D*). A comparable 20 kDa band was also detected when we used C-terminal tag antibody (Fig. S4). These findings suggests that a

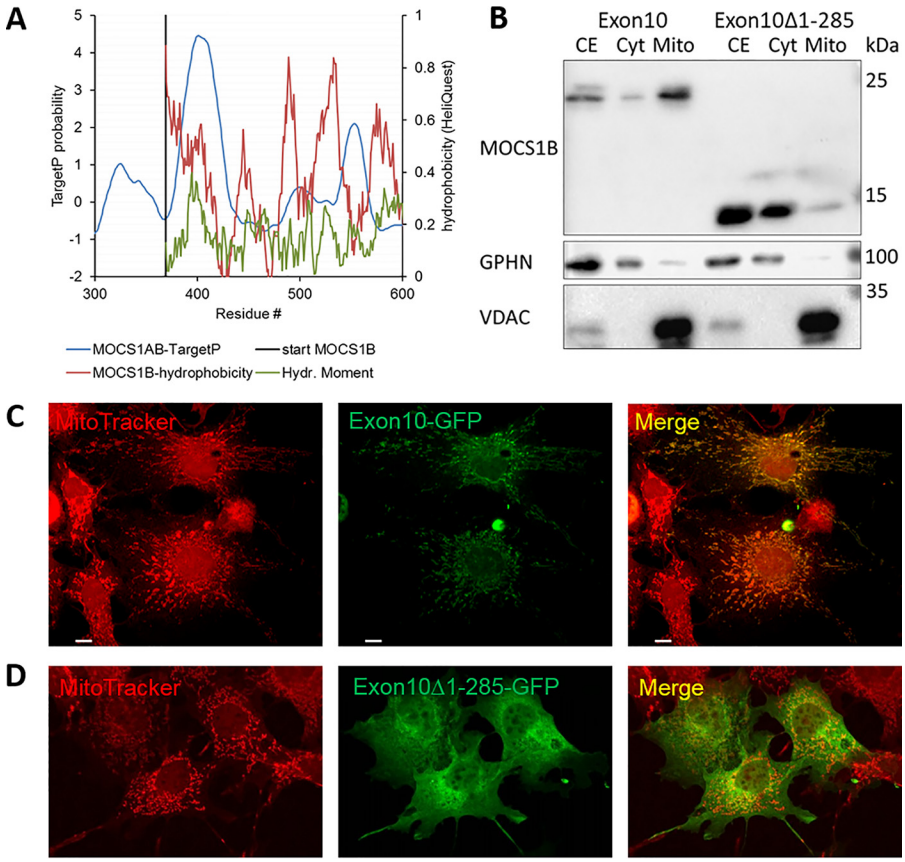

Figure 5. Identification of exon 10 encoded MOCS1B translocation signal. *A*, TargetP and HeliQuest *in silico* analysis of the MOCS1AB amino acid sequence showing the C-terminal residues 300 to 600. *B*, cellular fractionation of HEK293 cells transiently expressing the exon 10 encoded either full-length MOCS1B protein (26.6 kDa) or a truncated MOCS1B protein not containing the N-terminal 95 residues (16.8 kDa). The cells were fractionated and 10 μg of each fraction were loaded on a 12%SDS-PAGE (*CE*: crude extract; *Cyt*: cytosol; *Mito*: mitochondria). Subsequent Western blot analysis was performed using anti-MOCS1B, anti-gephyrin, and anti-VDAC antibodies. *C* and *D*, transient expression of (*C*) exon 10 and (*D*) exon 10Δ1–285 as GFP fusions in COS7 cells. Following 48 h of transient expression, mitochondria were stained with MitoTracker® Red CMXRos and analyzed by confocal laser scanning microscopy (three independent experiments). Overlay between the *red* and *green* (GFP) channel is shown in the *yellow* merge panel.

MOCS1B protein lacking the entire N-terminal MOCS1A domain, but not full-length MOCS1AB, was imported into the mitochondrial matrix. To provide further support for the exclusive localization of MOCS1B to the mitochondrial matrix, mitochondria were enriched from HEK293 cells overexpressing MOCS1AB-ad and exposed to an alkaline extraction of the mitochondrial membranes. As a consequence, the inner and outer mitochondrial membranes are separated from the soluble fractions consisting of the intermembrane space and the mitochondrial matrix. Subsequent Western blot analysis revealed an exclusive localization of full-length MOCS1AB to mitochondrial membranes whereas the proteolytically processed MOCS1B protein was mainly found in the soluble fraction, which was in line with the respective loading controls for IMS (sulfite oxidase) and outer membrane (VDAC) (Fig. 6*E*). Therefore the full-length MOCS1AB protein represents the premature protein of MOCS1B, which is proteolytically cleaved during procession to the mitochondrial matrix N-terminal to the MOCS1B domain, resulting in a mature soluble MOCS1B protein.

Given the surprising nature of this finding we subsequently aimed to further elucidate the cleavage of MOCS1AB. *In silico* analysis of the MOCS1B sequence using MitoFates (28) and MitoProt (21) revealed two different MPP cleavage sites of MOCS1AB (splice type III) at the positions 432 (MitoFates) and 437 (MitoProt). To demonstrate MPP cleavage at the corresponding position, the hypothesized MPP cleavage sites were disrupted by exchanging Arg-431 and Arg-436 to Trp, given that this type of substitution has been reported to abolish MPP cleavage (29). The constructs were expressed in HEK293 cells and Western blot analysis of enriched mitochondria revealed strongly reduced MPP cleavage of the R431W variant, whereas the R436W variant and the WT-MOCS1AB were cleaved (Fig. 6*F*). This finding strongly indicates that during MOCS1AB import MPP cleaves MOCS1AB at position 432, producing a 188 amino acid MOCS1B protein.

Discussion

In this study we were able to dissect the impact of alternative splicing of both exon 1 and exon 9 of *MOCS1* on the complex maturation path of MOCS1 proteins leading to the mitochondrial localization of MOCS1A and MOCS1B. The major impact of exon 9 splicing on MOCS1 proteins has been known for years (15), defining the expression of two different types of proteins, MOCS1A or MOCS1AB, respectively. The contribution of exon 1 splicing was not understood, except that exon 1d was found to be essential for catalytic activity as it contains two conserved cysteine residues required for the coordination of

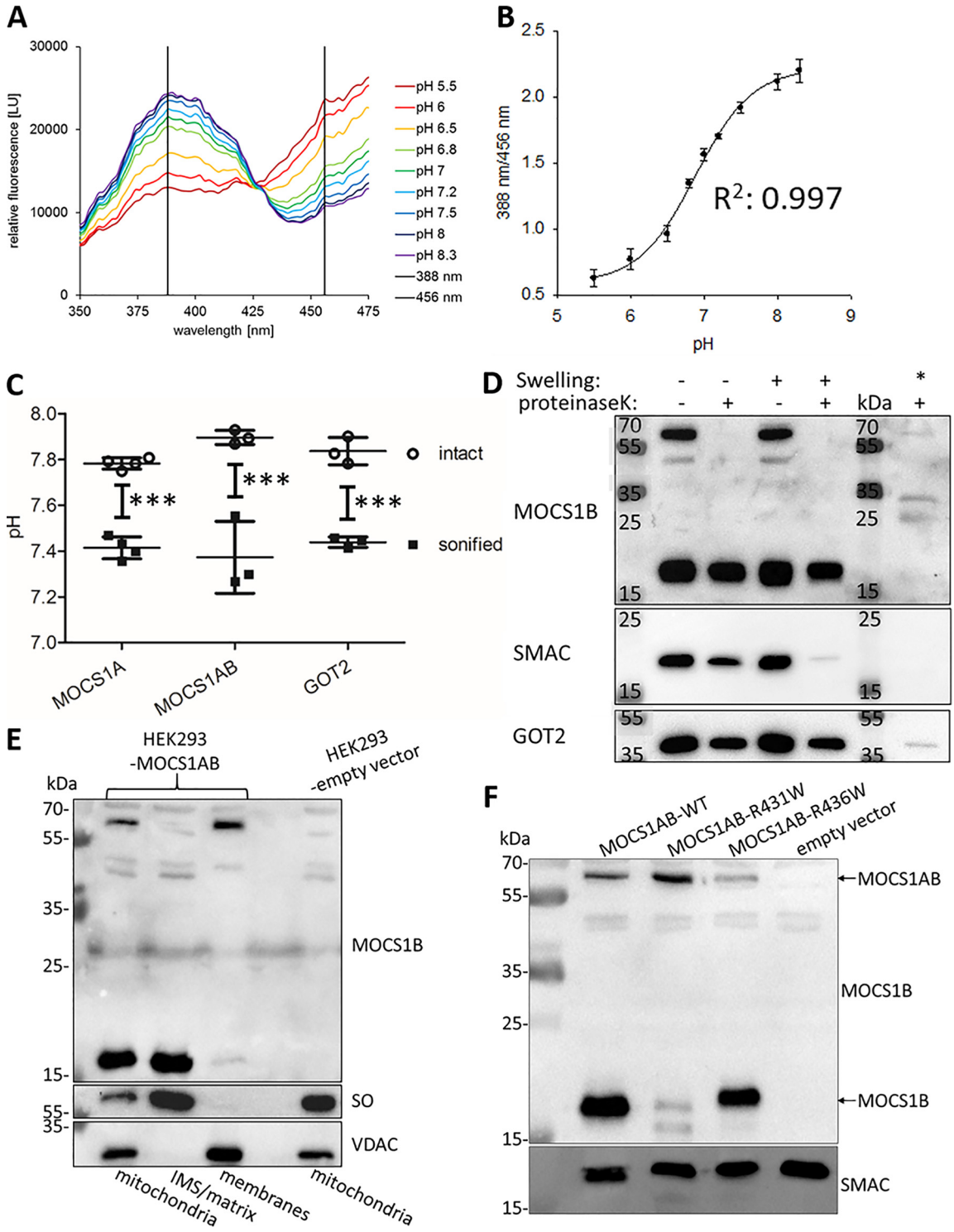

Figure 6. Submitochondrial localization of MOCS1AB proteins. *A–C*, excitation-scan measurements of enriched mitochondria from HEK293 cells transiently expressing MOCS1A-ad, MOCS1AB-bcd, or GOT2 as pHluorin fusions at 510 nm emission wavelength. *A*, MOCS1-ad excitation spectra of disrupted mitochondria in buffer of different known pH values. *B*, sigmoidal-fit calibration curve of pHluorin of the excitation maxima ratios (388 nm/456 nm) *versus* the pH values. Each point was measured as biological triplicate. *C*, fluorescence based pH-determination of intact mitochondria (*black bar*) and disrupted mitochondria (*gray bar*) using the pHluorin calibration curve. *D*, partial proteolysis experiment of mitochondria enriched from HEK293 cells overexpressing MOCS1AB-ad without tag (MOCS1AB: 68.3 kDa; MOCS1B: 19.8 kDa). One of each fraction of intact and swollen mitochondria were treated with proteinase K, as well as one additional sample of disrupted mitochondria (*, *right lane*). Subsequent 12% SDS-PAGE followed by Western blot analysis was performed using anti-MOCS1B, anti-SMAC, and anti-GOT2 antibodies. *E*, Western blot analysis of sub-fractionated HEK293 cells. Mitochondrial membranes and soluble mitochondrial fractions were separated by alkaline extraction and subsequent ultra-centrifugation. Successful separation was demonstrated using anti–sulfite oxidase and anti-VDAC antibodies. Unprocessed MOCS1AB and mature MOCS1B were visualized using anti-MOCS1B antibody. *F*, Western blot analysis of mitochondria (10 μg) enriched from HEK293 cells expressing MOCS1AB-ad–WT, MOCS1AB-ad–R431W, MOCS1AB-ad–R436W, and empty vector. Unprocessed MOCS1AB (68.3 kDa) and processed MOCS1B (19.8 kDa) were visualized using MOCS1B antibody. SMAC antibody was used as loading control.

the N-terminal [4Fe-4S] cluster. This cluster is crucial for catalytic function of MOCS1A as it is assumed to generate an adenosyl radical in the same way as MoaA in bacteria (11). This proposal is supported by complementation experiments of MoaA-deficient *E. coli* cells, demonstrating a loss of catalytic activity in the MOCS1A-a splice variant (Fig. S2).

Furthermore, we were able to show that exon 1a and exon 1b determine the cellular localization of MOCS1 proteins. Although exon 1a–encoded residues mediated translocation of MOCS1A to the mitochondrial matrix, MOCS1A proteins with an N-terminal extension encoded by exon 1b remained cytosolic. The function of exon 1c remains unknown; however, it should be considered that exons 1b–d are not separated by introns (18) but rather represent one exon which may be spliced partially, similar to exon 9. In either case, we observed that exon 1c is not essential for catalytic activity (Fig. S2) yet might stabilize the MOCS1A protein (Fig. S1).

Most surprisingly, we found that splicing of exon 9, which is known to produce either active MOCS1A or active MOCS1B protein, overrides the cytosolic translocation of the two discovered cytosolic splice variants, in respect to their N-terminal extension. This is a result of a sequence encoded by exon 10 representing a 95-residue linker region separating the conserved MOCS1A and MOCS1B domains, which is found in all type II and type III splice variants of MOCS1. This linker is facilitating import into the mitochondrial matrix and contains a mitochondrial peptidase cleavage site as witnessed in our translocation studies and proteolysis experiments and as observed in abolishment of MPP cleavage in the R431W variant. This cleavage site was predicted by MitoFates, whereas MitoProt recognized a MPP cleavage site downstream at position 437. Therefore it is remarkable that the R431W variant abolished the cleavage of MOCS1AB, because we would have suspected that MPP would still be able to cleave MOCS1AB at the downstream 437 position. However, creating a double Arg variant was not required for abolishment of MPP cleavage. This allows us to precisely map the cleavage site to position 432 (numbering according to splice type III-ad). The remaining MOCS1B protein (residues 433–620) has a calculated molecular mass of 19.8 kDa, exactly matching the observed size of the cleavage product. Consistently, the recombinantly expressed MOCS1B protein (missing the entire 95-residue linker region) was observed at 18.4 kDa, whereas the cleavage product was slightly larger because of the removal of only 64 N-terminal residues (Fig. S5).

Our findings promote the idea that ancestral *MOCS1A* and *MOCS1B* genes, both encoding their separate localization signals, were fused in vertebrates resulting in an internalization of the MOCS1B translocation signal. As a consequence, we favor the hypothesis of a TOM/TIM23-mediated import of MOCS1AB proteins (30). We furthermore found that exon 1 splicing does not impact MOCS1B procession as observed in partial proteolysis experiments of different MOCS1AB splice variants (Fig. S4). This is remarkable in light of the competing nature of the additional translocation signal present in MOCS1AB-a/ad variants, which in turn suggests a hierarchical import. The fate of the N-terminal MOCS1AB cleavage product consisting of MOCS1A (missing the catalytically essential C-terminal double glycine motif encoded by exon 9) remains unknown.

A very recently reported Moco deficiency type A patient case demonstrated that the expression of the MOCS1AB fusion protein is not strictly required for the biosynthetic activity of MOCS1 proteins. In this patient, low amounts (~1%) of MOCS1B protein (residues 425–620 according to splice type III numbering) were able to produce ~1% of WT Moco levels leading to a mild patient phenotype (31).

In humans, all four genes encoding for Moco synthetic proteins represent gene fusions (*MOCS1*, *MOCS2, MOCS3*, and *GPHN*). Although *MOCS2* encodes for a unique bicistronic mRNA with overlapping reading frames leading to the orchestrated expression of MOCS2A and MOCS2B proteins by a leaky scanning mechanism resulting in the assembly of the heterotetrameric MPT-synthase complex (8), *MOCS3* and *GPHN* encode for fusion proteins. MOCS3 is responsible for the reactivation of MOCS2A and harbors beside the NifS-like sulfurtransferase domain an additional rhodanese-like domain not present in prokaryotes (32). Gephyrin combines two catalytic activities that are represented by two different Moco synthetic proteins (MogA and MoeA) (33). Orchestrated expression of proteins catalyzing subsequent reaction steps results in the formation of hetero-oligomers or fusion proteins, which ensures equal expression levels of cooperating proteins (MOCS2) or catalytic domains (MOCS3, gephyrin). MOCS1 represents an example that goes beyond the functional interaction by ensuring orchestrated maturation of MOCS1A and MOCS1B.

In aggregate, biosynthesis of Moco is an evolutionary ancient pathway with each of its reaction steps representing a complex chemical transformation. In particular the reaction mechanism of cPMP formation represents a radical-based rearrangement reaction being entirely conserved in all kingdoms of life (1). Even though the underlying chemistry is highly conserved, the structures of the involved genes differ greatly. Tracking back the evolutionary event of the *MOCS1* gene fusion by aligning MoaA and MoaC in selected species revealed that the gene fusion was not just gained in ophisthokonta, but is a shared feature of the unikonta, given that the amoeba *Dictyostelium discoideum* harbors a fused *MOCS1* orthologue. Therefore the gene fusion event can be traced back to the unikonta/bikonta junction. Besides the above-discussed functional benefits of gene fusions in Moco biosynthesis, in the case of *MOCS3* and *GPHN* gene fusion served as evolutionary root for novel functions in higher eukaryotes (34, 35).

In conclusion, in this study we were able to demonstrate that MOCS1 proteins target to the mitochondrial matrix. We revealed the effects of alternative splicing on MOCS1 proteins allowing a first comprehensive understanding of the interplay of alternative splicing, cellular translocation, and proteolysis-mediated maturation of MOCS1 proteins.

Experimental procedures

Materials, plasmids, cell lines, and bacterial strains

Oligonucleotides for PCR and sequencing were purchased from Sigma. Restriction enzymes required were purchased

from Fermentas. The T5 RNA polymerase-based bacterial pQE-80L expression vector was used for expression of *MOCS1* splice variants in *E. coli* and purchased from Qiagen. Mammalian expression vectors used for localization studies in COS7 cells and expression in HEK293 cells were pEGPF-N1 and pcDNA3.1myc/His-A, were purchased from Invitrogen. The pHluorin-N1 vector was derived from pEGFP-N1. All cell lines were grown in DMEM containing fetal calf serum and L-glutamine (PAN^{TM}-Biotech) and were tested for mycoplasma contamination every 3 months. Bacterial strains *E. coli* WT MC4100 (*araD139 Δ(argF-lac)U169 rpsL150 relA1 flbB3501 deoC1 ptsF25 rbsR*) and *moaA*$^-$ and *moaC*$^-$ mutant strains (*F-thr, leu his pro arg thi ade gal lacY malE xyl ara mtl str Tr λr*) were used for complementation studies.

Cloning of MOCS1 splice variants

Constructs were derived from pRitaIX (kindly provided by J. Reiss, Goettingen) (36) whereas exon 1a was synthesized *in vitro* (GenScript). Based on the published gene sequences (16–18, 20), the different splice variants were obtained by two-step PCR reactions fusing the respective exons. Amino acid exchange variants of MOCS1 were created using site-directed mutagenesis. Therefore two PCR fragments were created harboring the mutation at the 3′ or 5′ end. Fragments were subsequently fused by PCR and fused products were inserted into the respective vector. The identities of all generated constructs were confirmed by sequencing (GATC-Biotech/Eurofins Genomics).

Transfection of COS7 and HEK293 cells and transient protein expression

COS7 and HEK293 cells were grown in DMEM supplemented with 10% fetal calf serum and L-glutamine. For transfection, cells were seeded into 12-well plates (40,000 cells/well) or 10-cm dishes (4.5×10^6 cells/dish), transfected with FuGENE (Promega) or polyethylenimine (Sigma), respectively, according to manufacturer's instructions. Transfected HEK293 cells were harvested and prepared for further analysis as described.

Fluorescence and co-localization analysis

COS7 cells were grown on collagen-coated coverslips, transfected with the respective transgene, and cultured for 24 h. Cells were washed with PBS and mitochondria were stained with MitoTracker® Red CMXRos according to the manufacturer's protocol. Following MitoTracker® Red staining, cells were washed twice with PBS and fixed with 4% paraformaldehyde. Coverslips were mounted on microscope slides using Mowiol (Calbiochem) with 1,4-diazabicyclo(2,2,2)-octane (DABCO, Merck) and dried at 37 °C overnight. Samples were subsequently randomly numbered and statistically analyzed by a person not involved in sample preparation (Fig. S6). GFP and MitoTracker® Red fluorescence was visualized by confocal laser scanning microscopy with Tι-Eclipse (Nikon).

Enrichment and sub-fractionation of mitochondria from transfected HEK293 cells

Mitochondria were enriched from HEK293 cells expressing the respective *MOCS1* splice variants using a modified previously described method (37). All fractions were sonicated for 30 s at 10% amplitude using a digital sonifier (Branson, Model 250-D) and centrifuged at 20,000 × *g* for 5 min at 4 °C before determination of protein concentration (Roti®-Quant; Roth, Germany) and supplementation with SDS loading buffer to remove protein aggregates. For partial proteolysis experiments enriched mitochondria were separated in 100 μg pellets, which were subsequently resuspended in 100 μl 10 mM HEPES buffer pH 7.6 containing 1 mM $CaCl_2$. For the samples of intact mitochondria the buffer additionally contained 220 mM mannitol and 70 mM sucrose. After 5 min incubation on ice the control sample was sonicated for 30 s at 10% amplitude and 2 μl of a 5 mg/ml proteinase K solution (Roth, Germany) were added to the respective samples (swollen and swollen + sonicated). After additional 10 min incubation on ice PMSF (final concentration 1 mM) was added and proteins were precipitated using TCA (final concentration 5%) for 10 min on ice.

Membrane and soluble mitochondrial proteins were fractionated by alkaline extraction. Therefore enriched mitochondria were resuspended in 0.1 M Na_2CO_3, pH 11.5. After 30 min incubation on ice, mitochondria were centrifuged at 70,000 × *g* for 1 h at 4 °C. Resulting pellets containing the mitochondrial membranes were washed with H_2O and resuspended in SDS loading buffer. The supernatants were concentrated using a 3 kDa cutoff protein concentrator and supplemented with SDS loading buffer.

Western blot analysis

Localization of proteins of fractionated HEK293 cells and sub-fractionated mitochondria was analyzed by Western blotting following SDS-PAGE and subsequent semi-dry blot. For the detection of MOCS1 proteins the following antibodies were used in the respective dilutions: anti-MOCS1A (rabbit polyclonal, Abcam, ab176989, 1/200), anti-MOCS1B (rabbit polyclonal, Eurogentec, rabbit SY7796, 1/100), anti–GFP-tag (rabbit polyclonal, Invitrogen, A6455, 1/1000), and anti-MYC-tag (mouse monoclonal, cell supernatant 9E10, 1/5). To ensure successful fractionation and sub-fractionation the following antibodies were used as controls: anti-GOT2 (rabbit polyclonal, Sigma, SAB2100–950, 1/500), anti-gephyrin (mouse monoclonal, cell supernatant 3B11, 1/20), anti-SMAC/Diablo (rabbit polyclonal, Abcam, ab8114, 1/2000), anti-sulfite oxidase (mouse monoclonal, Abcam, ab57852, 1/1000), and anti-VDAC1/Porin (rabbit polyclonal, Abcam, ab15895, 1/1000). All antibodies were diluted in TBST containing 2% dried nonfat milk powder. Western blotting membranes were analyzed using a ChemiDoc MP Imaging System (Bio-Rad) and the according software (ImageLab 5.2.1, Bio-Rad).

MOCS1B antibody

The MOCS1B domain (encoded by exon 10 Δ1–285) was expressed in *E. coli* BL21 as N-terminal His-tagged protein using a pQE80-L vector. Purification was achieved using nickel-nitrilotriacetic acid resin. The protein was eluted using a potassium phosphate pH 8.0 buffer containing NaCl and imidazole (250 mM). Subsequently the buffer was exchanged to a 20 mM Tris-HCl buffer pH 7.8 containing 200 mM NaCl using a PD10-column (GE Healthcare) and diluted to 10 mg/ml. Purity of the

protein was confirmed by a 12% SDS-PAGE using Coomassie Blue staining. The antibody was subsequently produced using the acquired protein as antigen (Eurogentec) and tested against different antigen concentrations (0.2–20 ng), as well as recombinantly expressed MOCS1AB from HEK293 cell extract.

Determination of intra-mitochondrial pH values

Mitochondria were enriched from HEK293 cells overexpressing the desired proteins as pHluorin fusions. For the determination of the pHluorin pK_a curves, pellets of enriched mitochondria were resuspended in water (2 mg/ml) and sonicated for 30 s at 10% amplitude. Subsequently, 100 μl extract were mixed with 100 μl 2× buffer (50 mM MES or Tris-HCl buffer pH 5.5–8.3, 0.3 M NaCl) and excitation spectra were recorded from 350 nm to 500 nm at an emission wavelength of 510 nm at room temperature using a microplate reader (Tecan InfiniteM200). To measure the pH values of pHluorin fusions in intact mitochondria, pellets of enriched mitochondria were resuspended in buffer (pH 7.4 at 37 °C; 1 mg enriched mitochondria/ml) and fluorescence was immediately determined as described above, but at 37 °C. Subsequently, each sample was sonicated for 30 s (10% amplitude) and remeasured.

Determination of cPMP and MPT content

cPMP was detected as Compound Z in crude cell extracts as described (7). In brief, protein extracts (0.5 mg total protein) were oxidized, purified by quaternary aminoethyl column chromatography and HPLC analysis (Agilent Technologies) was performed using a C18-reversed phase column (Waters). Elution from quaternary aminoethyl columns was performed with 50 mM HCl. cPMP concentrations were expressed in picomoles of compound Z per milligram of total protein. All determinations were performed as biological triplicates ($n = 3$).

Statistics

If not stated otherwise, all numerical data were reported as mean ± S.D. All measurements were performed at least in triplicates. Statistical analysis (unpaired *t* test) was performed with SigmaPlot (Systat Software Inc.). Significance levels are indicated in figures as *, $p < 0.05$; **, $p < 0.01$; ***, $p < 0.001$.

Author contributions—S. J. M., J. R., and G. S. conceptualization; S. J. M. and J. R. data curation; S. J. M. and J. R. formal analysis; S. J. M. and G. S. funding acquisition; S. J. M., J. R., and G. S. validation; S. J. M., J. R., and G. S. investigation; S. J. M. and J. R. visualization; S. J. M. and J. R. methodology; S. J. M., J. R., and G. S. writing-original draft; S. J. M., J. R., and G. S. writing-review and editing; G. S. resources; G. S. supervision; G. S. project administration.

Acknowledgments—We are grateful to Monika Laurien (University of Cologne, Germany) for technical assistance. We thank Dr. Jochen Reiss (University of Goettingen) for providing the plasmid pRITAIX and Prof. Reinhart Krämer for providing the pHluorin sequence. We thank Prof. Johannes Hermann and Prof. Timo Mühlhaus for the iMTS-L propensity analysis.

References

1. Schwarz, G., Mendel, R. R., and Ribbe, M. W. (2009) Molybdenum cofactors, enzymes and pathways. *Nature* **460,** 839–847 CrossRef Medline
2. Schwarz, G. (2005) Molybdenum cofactor biosynthesis and deficiency. *Cell Mol. Life Sci.* **62,** 2792–2810 CrossRef Medline
3. Schwahn, B. C., Van Spronsen, F. J., Belaidi, A. A., Bowhay, S., Christodoulou, J., Derks, T. G., Hennermann, J. B., Jameson, E., König, K., McGregor, T. L., Font-Montgomery, E., Santamaria-Araujo, J. A., Santra, S., Vaidya, M., Vierzig, A., *et al.* (2015) Efficacy and safety of cyclic pyranopterin monophosphate substitution in severe molybdenum cofactor deficiency type A: A prospective cohort study. *Lancet* **386,** 1955–1963 CrossRef Medline
4. Veldman, A., Santamaria-Araujo, J. A., Sollazzo, S., Pitt, J., Gianello, R., Yaplito-Lee, J., Wong, F., Ramsden, C. A., Reiss, J., Cook, I., Fairweather, J., and Schwarz, G. (2010) Successful treatment of molybdenum cofactor deficiency type A with cPMP. *Pediatrics* **125,** e1249–e1254 CrossRef Medline
5. Santamaria-Araujo, J. A., Fischer, B., Otte, T., Nimtz, M., Mendel, R. R., Wray, V., and Schwarz, G. (2004) The tetrahydropyranopterin structure of the sulfur-free and metal-free molybdenum cofactor precursor. *J. Biol. Chem.* **279,** 15994–15999 CrossRef Medline
6. Kuper, J., Llamas, A., Hecht, H. J., Mendel, R. R., and Schwarz, G. (2004) Structure of the molybdopterin-bound Cnx1G domain links molybdenum and copper metabolism. *Nature* **430,** 803–806 CrossRef Medline
7. Hänzelmann, P., Schwarz, G., and Mendel, R. R. (2002) Functionality of alternative splice forms of the first enzymes involved in human molybdenum cofactor biosynthesis. *J. Biol. Chem.* **277,** 18303–18312 CrossRef Medline
8. Reiss, J., Dorche, C., Stallmeyer, B., Mendel, R. R., Cohen, N., and Zabot, M. T. (1999) Human molybdopterin synthase gene: Genomic structure and mutations in molybdenum cofactor deficiency type B. *Am. J. Hum. Genet.* **64,** 706–711 CrossRef Medline
9. Wuebbens, M. M., Liu, M. T., Rajagopalan, K., and Schindelin, H. (2000) Insights into molybdenum cofactor deficiency provided by the crystal structure of the molybdenum cofactor biosynthesis protein MoaC. *Structure* **8,** 709–718 CrossRef Medline
10. Hänzelmann, P., Hernández, H. L., Menzel, C., García-Serres, R., Huynh, B. H., Johnson, M. K., Mendel, R. R., and Schindelin, H. (2004) Characterization of MOCS1A, an oxygen-sensitive iron-sulfur protein involved in human molybdenum cofactor biosynthesis. *J. Biol. Chem.* **279,** 34721–34732 CrossRef Medline
11. Hover, B. M., and Yokoyama, K. (2015) C-terminal glycine-gated radical initiation by GTP 3′,8-cyclase in the molybdenum cofactor biosynthesis. *J. Am. Chem. Soc.* **137,** 3352–3359 CrossRef Medline
12. Hover, B. M., Tonthat, N. K., Schumacher, M. A., and Yokoyama, K. (2015) Mechanism of pyranopterin ring formation in molybdenum cofactor biosynthesis. *Proc. Natl. Acad. Sci. U.S.A.* **112,** 6347–6352 CrossRef Medline
13. Reiss, J., Christensen, E., Kurlemann, G., Zabot, M. T., and Dorche, C. (1998) Genomic structure and mutational spectrum of the bicistronic MOCS1 gene defective in molybdenum cofactor deficiency type A. *Hum. Genet.* **103,** 639–644 CrossRef Medline
14. Lu, Y., Zhang, Y., Hang, X., Qu, W., Lubec, G., Chen, C., and Zhang, C. (2013) Genome-wide computational identification of bicistronic mRNA in humans. *Amino Acids* **44,** 597–606 CrossRef Medline
15. Gray, T. A., and Nicholls, R. D. (2000) Diverse splicing mechanisms fuse the evolutionarily conserved bicistronic MOCS1A and MOCS1B open reading frames. *RNA* **6,** 928–936 CrossRef Medline
16. Reiss, J., Cohen, N., Dorche, C., Mandel, H., Mendel, R. R., Stallmeyer, B., Zabot, M. T., and Dierks, T. (1998) Mutations in a polycistronic nuclear gene associated with molybdenum cofactor deficiency. *Nat. Genet.* **20,** 51–53 CrossRef Medline
17. Arenas, M., Fairbanks, L. D., Vijayakumar, K., Carr, L., Escuredo, E., and Marinaki, A. M. (2009) An unusual genetic variant in the MOCS1 gene leads to complete missplicing of an alternatively spliced exon in a patient with molybdenum cofactor deficiency. *J. Inherit. Metab. Dis.* **32,** 560–569 CrossRef Medline
18. Gross-Hardt, S., and Reiss, J. (2002) The bicistronic MOCS1 gene has alternative start codons on two mutually exclusive exons. *Mol. Genet. Metab.* **76,** 340–343 CrossRef Medline

19. Teschner, J., Lachmann, N., Schulze, J., Geisler, M., Selbach, K., Santamaria-Araujo, J., Balk, J., Mendel, R. R., and Bittner, F. (2010) A novel role for *Arabidopsis* mitochondrial ABC transporter ATM_3 in molybdenum cofactor biosynthesis. *Plant Cell* **22,** 468–480 CrossRef Medline
20. Reiss, J., and Hahnewald, R. (2011) Molybdenum cofactor deficiency: Mutations in GPHN, MOCS1, and MOCS2. *Hum. Mutat.* **32,** 10–18 CrossRef Medline
21. Claros, M. G., and Vincens, P. (1996) Computational method to predict mitochondrially imported proteins and their targeting sequences. *Eur. J. Biochem.* **241,** 779–786 CrossRef Medline
22. Gautier, R., Douguet, D., Antonny, B., and Drin, G. (2008) HELIQUEST: A web server to screen sequences with specific α-helical properties. *Bioinformatics* **24,** 2101–2102 CrossRef Medline
23. Ciofi-Baffoni, S., Nasta, V., and Banci, L. (2018) Protein networks in the maturation of human iron-sulfur proteins. *Metallomics* **10,** 49–72 CrossRef Medline
24. Emanuelsson, O., Nielsen, H., Brunak, S., and von Heijne, G. (2000) Predicting subcellular localization of proteins based on their N-terminal amino acid sequence. *J. Mol. Biol.* **300,** 1005–1016 CrossRef Medline
25. Backes, S., Hess, S., Boos, F., Woellhaf, M. W., Gödel, S., Jung, M., Mühlhaus, T., and Herrmann, J. M. (2018) Tom70 enhances mitochondrial preprotein import efficiency by binding to internal targeting sequences. *J. Cell Biol.* **217,** 1369–1382 CrossRef Medline
26. Miesenböck, G., De Angelis, D. A., and Rothman, J. E. (1998) Visualizing secretion and synaptic transmission with pH-sensitive green fluorescent proteins. *Nature* **394,** 192–195 CrossRef Medline
27. Paroutis, P., Touret, N., and Grinstein, S. (2004) The pH of the secretory pathway: Measurement, determinants, and regulation. *Physiology* (*Bethesda*) **19,** 207–215 CrossRef Medline
28. Fukasawa, Y., Tsuji, J., Fu, S. C., Tomii, K., Horton, P., and Imai, K. (2015) MitoFates: Improved prediction of mitochondrial targeting sequences and their cleavage sites. *Mol. Cell Proteomics* **14,** 1113–1126 CrossRef Medline
29. Hartmann, B., Wai, T., Hu, H., MacVicar, T., Musante, L., Fischer-Zirnsak, B., Stenzel, W., Graf, R., van den Heuvel, L., Ropers, H. H., Wienker, T. F., Hubner, C., Langer, T., and Kaindl, A. M. (2016) Homozygous YME1L1 mutation causes mitochondriopathy with optic atrophy and mitochondrial network fragmentation. *Elife* **5,** e16078 CrossRef Medline
30. Kang, Y., Fielden, L. F., and Stojanovski, D. (2018) Mitochondrial protein transport in health and disease. *Semin. Cell Dev. Biol.* **76,** 142–153 CrossRef Medline
31. Mayr, S. J., Sass, J. O., Vry, J., Kirschner, J., Mader, I., Hövener, J. B., Reiss, J., Santamaria-Araujo, J. A., Schwarz, G., and Grünert, S. C. (2018) A mild case of molybdenum cofactor deficiency defines an alternative route of MOCS1 protein maturation. *J. Inherit. Metab. Dis.* **41,** 187–196 CrossRef Medline
32. Matthies, A., Rajagopalan, K. V., Mendel, R. R., and Leimkühler, S. (2004) Evidence for the physiological role of a rhodanese-like protein for the biosynthesis of the molybdenum cofactor in humans. *Proc. Natl. Acad. Sci. U.S.A.* **101,** 5946–5951 CrossRef Medline
33. Belaidi, A. A., and Schwarz, G. (2013) Metal insertion into the molybdenum cofactor: Product-substrate channelling demonstrates the functional origin of domain fusion in gephyrin. *Biochem. J.* **450,** 149–157 CrossRef Medline
34. Jüdes, A., Ebert, F., Bär, C., Thüring, K. L., Harrer, A., Klassen, R., Helm, M., Stark, M. J., and Schaffrath, R. (2015) Urmylation and tRNA thiolation functions of ubiquitin-like Uba4.Urm1 systems are conserved from yeast to man. *FEBS Lett.* **589,** 904–909 CrossRef Medline
35. Fritschy, J. M., Harvey, R. J., and Schwarz, G. (2008) Gephyrin: Where do we stand, where do we go? *Trends Neurosci.* **31,** 257–264 CrossRef Medline
36. Kügler, S., Hahnewald, R., Garrido, M., and Reiss, J. (2007) Long-term rescue of a lethal inherited disease by adeno-associated virus-mediated gene transfer in a mouse model of molybdenum-cofactor deficiency. *Am. J. Hum. Genet.* **80,** 291–297 CrossRef Medline
37. Mattiazzi, M., D'Aurelio, M., Gajewski, C. D., Martushova, K., Kiaei, M., Beal, M. F., and Manfredi, G. (2002) Mutated human SOD1 causes dysfunction of oxidative phosphorylation in mitochondria of transgenic mice. *J. Biol. Chem.* **277,** 29626–29633 CrossRef Medline